Inhibition of photocatalysis of rutile nanoparticles via surface encrustation with La(OH)$_3$ quantum dots.

Nuwangi P Cooray[a], Rajib Chandra Das[a,b], Philip J Barker[c], Michael Lerch[d], Jung Ho Kim[a], Konstantin Konstantinov[a]*

a Institute for Superconducting and Electronic Materials, Faculty of Engineering and Information Sciences, University of Wollongong Innovation Campus, Squires Way, North Wollongong, NSW 2500, Australia

b Illawarra Health and Medical Research Institute, Wollongong, New South Wales 2522, Australia

c School of Chemistry and Molecular Bioscience, Faculty of Science, Medicine and Health, University of Wollongong, Wollongong, NSW 2522, Australia

d Centre for Medical Radiation Physics, School of Physics, Faculty of Engineering and Information Sciences, University of Wollongong, Wollongong, NSW 2522, Australia

Characterisation techniques

X-ray diffraction was used to identify the phase of the produced and commercial nanopowders using PANalytical Aeris XRD using Cu Kα (λ=1.54059 Å) radiation source.

Nanoparticle morphology, crystal characterisation and size were studied using JEOL JSM-7500 for Scanning Electron Microscopy (SEM) and JEOL ARM-200F for Scanning Transmission Electron Microscopy and Energy Dispersive Spectroscopy analysis (STEM and EDS).

The surface composition of the product nanocomposites was evaluated via x-ray photoelectron spectroscopy (XPS) using SPECS PHOIBOS 100 Analyzer installed in a high vacuum chamber with a base pressure below 10^{-8} mbar. X-ray excitation was provided by Al Kα radiation with a photon energy of 1486.6eV at a high voltage of 12 kV and power 120 W. The XPS binding energy spectra were recorded with the pass energy 20 eV in the fixed analyser transmission mode. The Analysis of the XPS data was carried out using CasaXPS 2.3.15 and Origin Pro software.

The surface area of all the materials was investigated using TriStar II (Micromeritics Instrument Corporation) surface area and porosity analyser. ~100 mg of sample was weighed into a glass sample tube and was placed in VacPrepTM 061 (Micromeritics Instrument Corporation) to degas under vacuum overnight at 120 °C to remove and adsorbed water and gas contaminants. Finally, the tubes were placed in the analyser and Brunauer Emmett-Teller (BET) measurements were taken using nitrogen (N$_2$) as the adsorbate gas with a cross-sectional area of 0.162 nm^2 at 77 K.

Thermogravimetric analysis (Perkin Elmer STA-6000) was carried out over a range of 30 °C to 900 °C at a heating rate of 5 °C.min^{-1} in air flow rate 20 ml.min^{-1} with an isothermal-period at 450 °C for 2 h. The weight loss of the materials with increasing temperature was assessed.

The Zeta potentials of the bare TiO_2 nanoparticles and nanocomposites dispersed in ethanol were measured using the Malvern Panalytical Zetasizer nano instrument, which determines the electrophoretic mobility of the particles and calculates the zeta potential.

Fluorescence spectra of the UV filter materials were obtained using Horiba Fluorolog FL3-221 to understand the energy dissipation pathway of TiO_2 and composite samples using an excitation wavelength of 340nm.

The UV absorbance of the samples was measured over the range of 800 to 200 nm using a Shimadzu UV-3600 spectrometer from Shimadzu Corporation (Kyoto, Japan) fitted with an integrating sphere. The nanoparticle suspensions were prepared in ethanol at 25 ppm concentration. The bandgap was determined using equation (1):

$$(\alpha h\nu)^n = A(h\nu - E_g) \hspace{3cm} (1)$$

Where, α is the absorption coefficient, h- Planck constant, ν- light frequency, A - a constant, and E_g the band gap. The value of n depends on the type of optical transition of a semiconductor (i.e., n = 2 for a direct transition and n = 0.5 for an indirect transition). The band gap can be estimated from a plot of $(\alpha h\nu)^n$ vs. the energy (hν).

The photocatalytic activity of the materials was evaluated by observing Crystal Violet (CV) dye degradation by the generation of Reactive Oxygen Species (ROS) from nanoparticles upon exposure to Ultraviolet (UV) radiation in an RPR-200 photochemical reactor (Rayonet, Branford, CT, USA) fitted with 300 nm and 350 nm Hg lamps. A solution of 5 ppm CV was stirred with 5 ppm nanocomposite sample under test and exposed to UV over 1hr, with an aliquot removed every 10 mins. The degradation of the dye was evaluated by measuring the intensity of the CV absorption maximum at 590nm, which correlates to the remaining dye concentration. The apparent rate constant k was calculated according to equation (2):

$$C_t = C_0 e^{-kt} \hspace{3cm} (2)$$

Where C_t is the concentration of the dye at time t and C_0 is the initial dye concentration.

Results

La(OH)$_3$ sample was separately prepared by conventional precipitation as described in the manuscript. The XRD pattern presented in Figure S1 (a) for La(OH)$_3$ matched with ICDD reference 04-005-8687 shows broad peaks, indicating the smaller crystallite size of La(OH)$_3$ QDs, which was calculated using
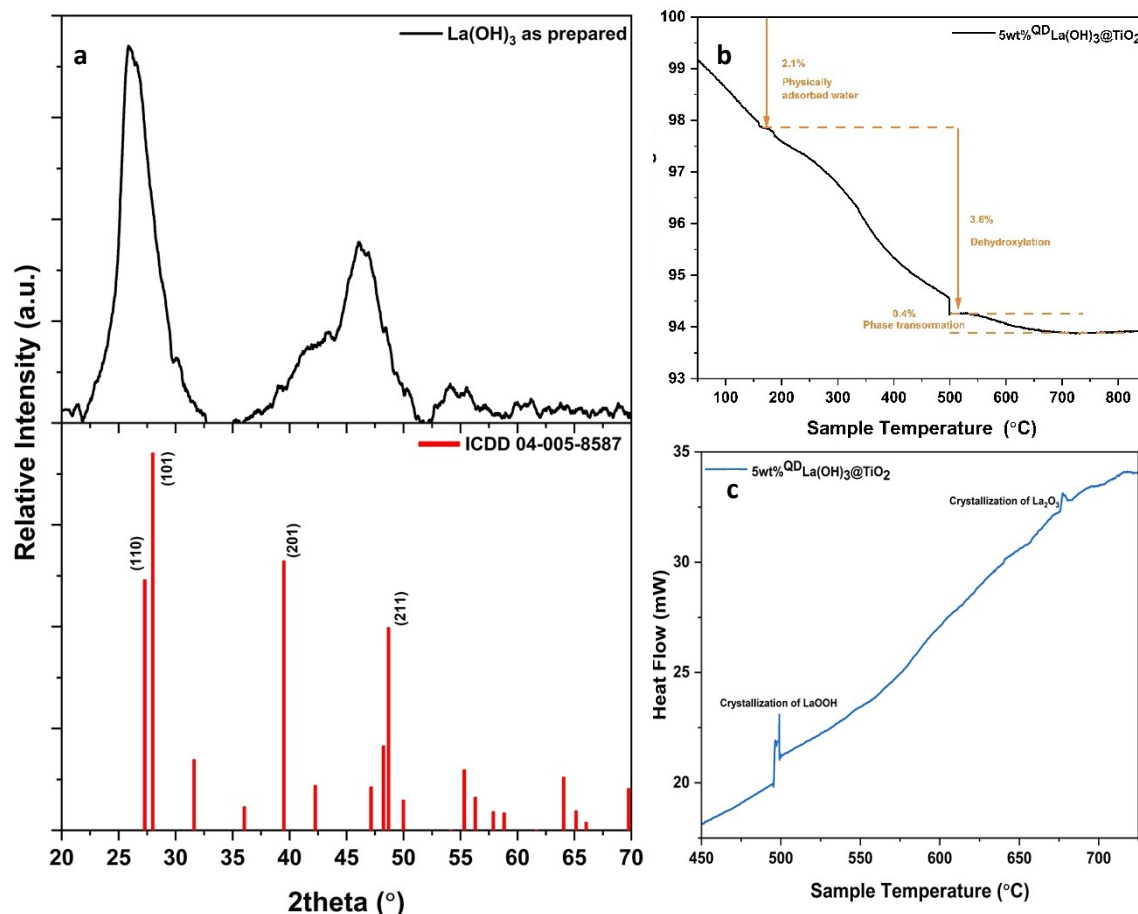

Figure S1 (a) XRD pattern of synthesised La(OH)$_3$ quantum dots and (b) TGA (c) DSC analysis of 5wt%^{QD}La(OH)$_3$@TiO$_2$

the Scherrer equation to be 3.2 ± 0.8nm.

Furthermore, the TGA (Thermogravimetric Analysis) curve of 5%wt ^{QD}La(OH)$_3$@TiO$_2$ in Figure S1 (b) shows a gradual decrease up to 200°C due to physical adsorbed water loss. Up to 500°C, dehydroxylation of La(OH)$_3$ and transformation into LaOOH occurs. A minor weight loss between 500-700 °C could be attributed to a phase transformation or further de-hydroxylation, possibly forming La$_2$O$_3$[1]. After 700°C, the curve flattens out, indicating that the material has stabilised. This is expected as the rutile phase of TiO$_2$ is thermally stable. In the DSC (Differential Scanning Calorimetry) presented in Figure S1 (c), a sharp peak around 500°C indicates an endothermic process corresponding to the crystallisation of LaOOH. The peak around 675°C represents a weak endothermic process associated with the crystallisation of La$_2$O$_3$[2,3]. The presence of TiO$_2$ likely influences the thermal behaviour of

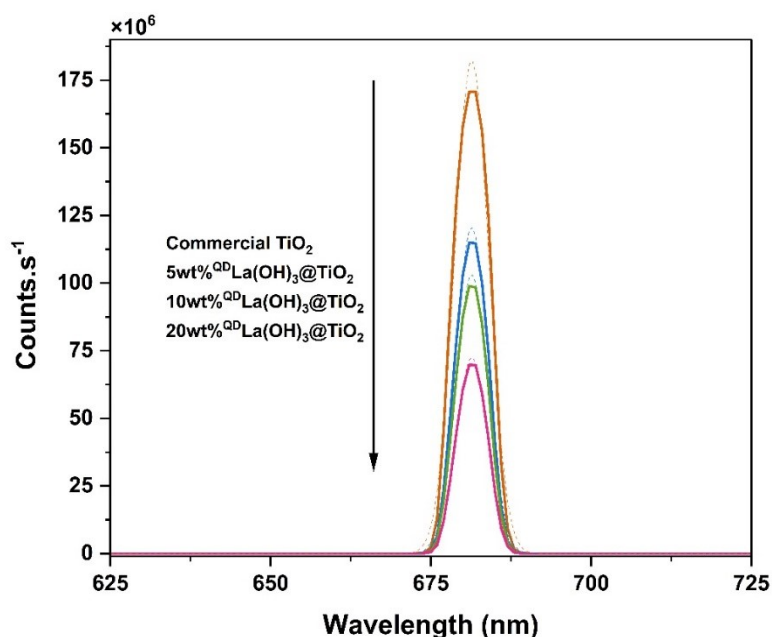La(OH)$_3$, as evidenced by the relatively high temperatures for crystallisation, making La(OH)$_3$ thermally

Figure S2 Fluorescence spectra of the TiO$_2$ and La(OH)$_3$@TiO$_2$ series monitored at an excitation wavelength of 340 nm

stable at room temperature in the composite.

According to the fluorescence spectra in Figure S2, the composite samples show decreased intensity in the fluorescence peak for TiO$_2$ with the increased amount of La(OH)$_3$ in the sample. Furthermore, adding ^{QD}La(OH)$_3$ to TiO$_2$ causes a slight shift in the emission peak towards a longer wavelength (red shift), as presented below in Table S1.

Table S1 Fluorescence peak emission wavelengths for commercial TiO$_2$ and ^{QD}La(OH)$_3$@TiO$_2$ composites at the excitation wavelength of 340nm

Sample	Fluorescence peak (nm)	Peak Intensity (×10^6 Counts.s^{-1})
Commercial TiO$_2$	681.383±0.013	182.36±0.79
5wt% ^{QD}La(OH)$_3$@TiO$_2$	681.394±0.008	120.69±0.34
10wt% ^{QD}La(OH)$_3$@TiO$_2$	681.395±0.007	103.23±0.26
20wt% ^{QD}La(OH)$_3$@TiO$_2$	681.422±0.006	72.67±0.15

This indicates that the surface encrustation with La(OH)$_3$ may induce fluorescence quenching effects, which can deactivate the excited state of TiO$_2$, inhibiting photocatalysis[4].

Transmission Electron Microscopy (TEM) images presented in Figure S3 show Bright field (BF) images (top) and High-angle annular dark-field (HAADF) images (bottom) of 10wt% ^{QD}La(OH)$_3$@TiO$_2$ composite. The formation of La(OH)$_3$ QDs is better identified in HAADF images since La has a higher atomic number (57) than Ti (22), and areas where La is present in the sample appear brighter in the HAADF images.
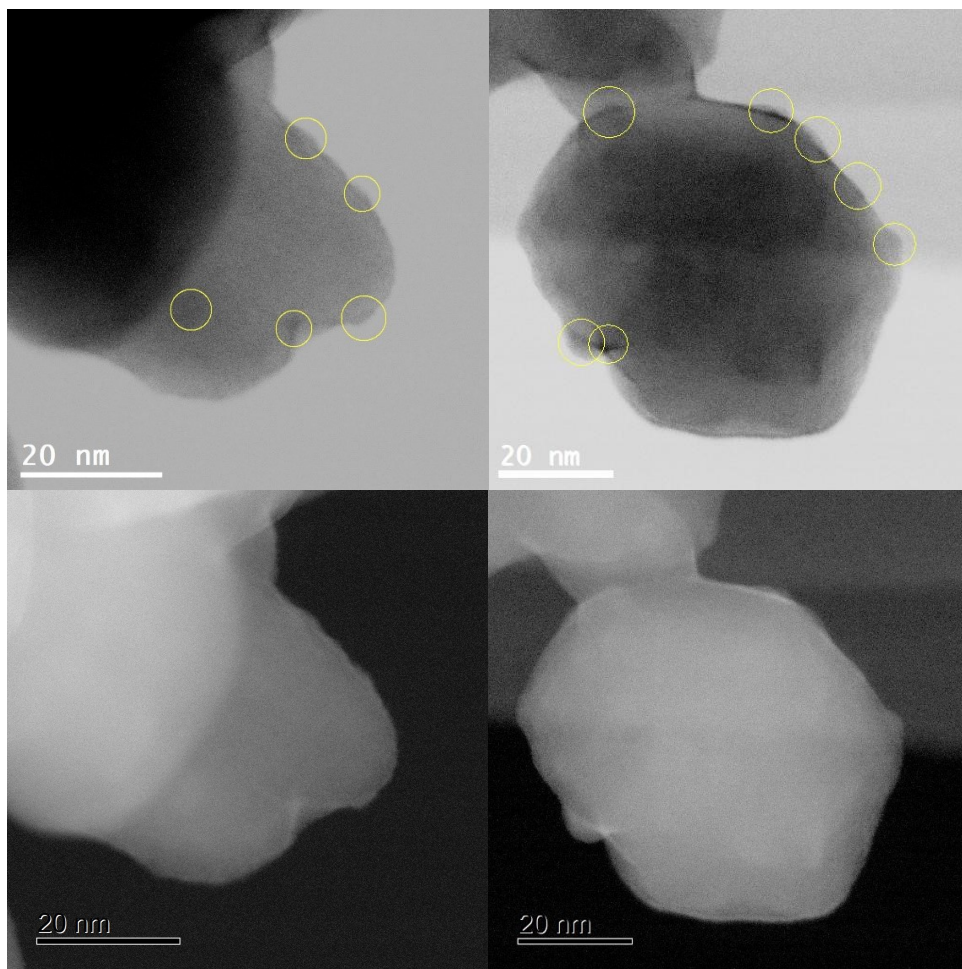

Figure S3 (top) BF and (bottom) HAADF images of 10wt%^{QD}La(OH)$_3$@TiO$_2$

Consequently, Figure S4 presents the EDS Energy Dispersive Spectroscopy (EDS) mapping of 10wt% ^{QD}La(OH)$_3$@TiO$_2$ sample. The images show La(OH)$_3$ is attached to the TiO$_2$ surface without fully coating the particle surface.

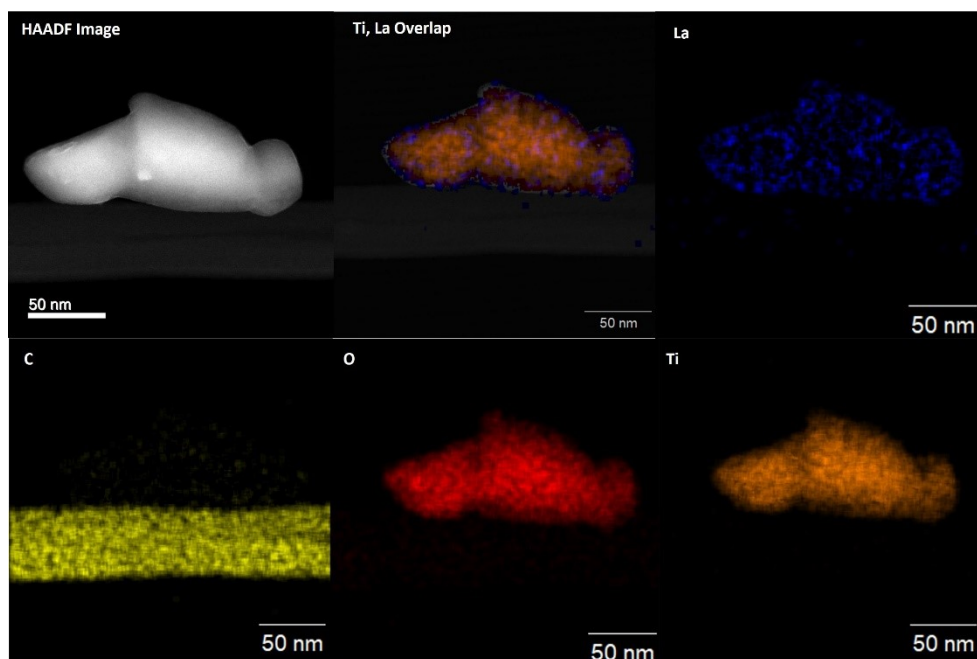**Figure S4 EDS mapping for 10wt% ^{QD}La(OH)$_3$@TiO$_2$ sample showing the elemental distribution of Ti, C, O and La**

The assessment of phototoxicity of the materials, cell viability assays with HaCaT have been performed in the presence of simulated sunlight for 5 min as presented in Figure S5. At low concentrations, the TiO$_2$ (rutile) nanoparticles tested here provided protection against UV radiation. At higher concentrations, photocatlysis prevails and cell viability is significantly reduced. On the other hand, with 10wt% nanocomposites, cell viability does not significantly change with concentration.

References

(1) J. -G. Kang, Y. -I. Kim, D. Won Cho, Y. Sohn, *Materials Science in Semiconductor Processing* **2015**, *40*, 737–743.
(2) A. Neumann, D. Walter, *Thermochimica Acta* **2006**, *445* (2), 200–204.
(3) M. Méndez, J. J. Carvajal, L. F. Marsal, P. Salagre, M. Aguiló, F. Díaz, P. Formentín, J. Pallarès, Y. Cesteros, *J Nanopart Res* **2013**, *15* (3), 1479
(4) S. C. Lee, N. Hasan, H.O. Lintang, M. Shamsuddin, L. Yuliati, *IOP Conf. Ser.: Mater. Sci. Eng.* **2016**, *107* (1), 012012.
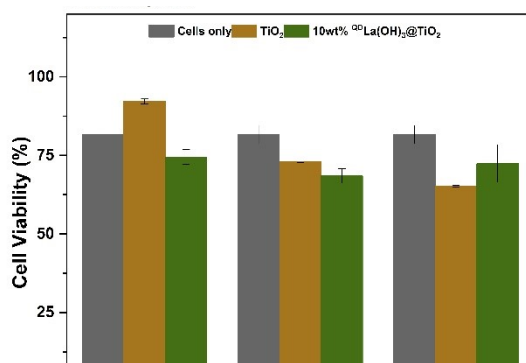
Figure S5 Average HaCaT cell viability upon 5 min simulated solar irradiation, expressed as percentage of viable cells with respect to IC$_0$ control (no UV) with TiO$_2$ (rutile) and 10wt% ^{QD}La(OH)$_3$@TiO$_2$ at 25, 50 and 100 mgL^{-1}.